Robotica (2017) volume 35, pp. 2018–2035. © Cambridge University Press 2016
doi:10.1017/S0263574716000692

Kinematics and inverse dynamics analysis for a novel 3-PUU parallel mechanism

Wang Liping, Xu Huayang and Guan Liwen*

Department of Mechanical Engineering, Tsinghua University, Beijing 100084, China

(Accepted September 10, 2016. First published online: November 24, 2016)

SUMMARY

The modules of parallel tool heads with 2R1T degrees of freedom (DOFs), i.e., two rotational DOFs and one translational DOF, have become so important in the field of machine tools that corresponding research studies have attracted extensive attention from both academia and industry. A 3-PUU (P represents a prismatic joint, U represents a universal joint) parallel mechanism with 2R1T DOFs is proposed in this paper, and a detailed discussion about its architecture, geometrical constraints, and mobility characteristics is presented. Furthermore, on the basis of its special geometrical constraint, we derive and explicitly express the parasitic motion of the 3-PUU mechanism. Then, the inverse kinematics problem, the Jacobian matrix calculation and the forward kinematics problem are also investigated. Finally, with a simplified dynamics model, the inverse dynamics analysis for the mechanism is carried out with the Principle of Virtual Work, and corresponding results are compared with that of the 3-PRS mechanism. The above analyses illustrate that the 3-PUU parallel mechanism has good dynamics features, which validates the feasibility of applying this mechanism as a tool head module.

KEYWORDS: Parallel mechanism, 3-PUU, 2R1T DOFs, kinematics analysis, dynamics analysis.

1. Introduction

Owing to its virtues including compact structure, high stiffness to weight ratio and good dynamics performance, parallel kinematic mechanisms (PKMs) have attracted widespread attention from both academia and industry. In the past decades, significant improvements have been made to PKMs. On the one hand, the emergence of academic fruits,[1–3] such as novel synthesis and design theories, new kinematics and dynamics performance indexes for analysis and optimization, high-effective control strategies etc., has provided solid theoretical support for the development of PKMs. On the other hand, a number of parallel manipulators have obtained practical applications in industry, presenting satisfying behavior, e.g., the Sprint Z3 tool head for metal machining,[4] the Delta robot for goods sorting,[5] the Stewart mechanism for spacecraft docking,[6] etc.

The high degree of stiffness and low inertia characteristics of parallel kinematic mechanism make it suitable for high-speed machine tools. Most of 6-degrees of freedom (DOFs) pure PKMs employ the Stewart–Gough architecture. However, 6-DOF parallel mechanisms suffer from shortcomings such as unsatisfactory workspace, poor orientation capability, and use of spherical joints that are difficult to manufacture. To overcome these defects, Tsai[7] proposed a new class of machines known as the hybrid kinematic machines (HKMs). HKM denotes a machine that serially connects a serial kinematic mechanism and a low-mobility PKM, and they collectively realize the required DOFs for machining. In the last decades, a great number of parallel mechanisms with 2R1T DOFs have been proposed and some of them were utilized as machine tool heads. The 3-PRS architecture (P represents an active prismatic joint, R and S represent a revolute joint and a spherical joint, respectively), based on which the Sprint Z3 tool head[4] was developed, is one of the most well-known mechanisms used in the HKMs field. A great deal of effort has been devoted to this mechanism, such as kinematics and dynamics analysis,[8–10] dimension synthesis and layout optimization,[11,12] and the design of its

* Corresponding author. E-mail: guanlw@mail.tsinghua.edu.cn

variants.[13,14] Due to 3-PRS mechanism's requirements on precise spherical joints, which are difficult and costly to manufacture, HKMs with 3-PRS mechanisms have not been widely used in developing countries until now. A3 tool head[15] is another famous parallel module designed for HKMs, behind which is the 3-RPS architecture. Comparison studies about Z3 and A3 have been carried out.[16] Besides, both 3-PRS and 3-RPS mechanism have inherent parasitic motions along the x- and y-axes of the fixed frame, and numerous 2R1T parallel architectures without parasitic motions have also been proposed.[17,18]

This paper proposes a novel 3-PUU architecture (U represents a universal joint) with 2R1T DOFs. It must be noted that there was a type of PKM named 3-PUU,[7,19–23] and it has even obtained widespread application in practice. However, the previous 3-PUU mechanism has three pure translational DOFs and was utilized as the position mechanism for an HKM. Instead, the 3-PUU mechanism presented in this paper owns two rotational DOFs and one translational DOF. Just like the 3-PRS mechanism, it can undertake orientation tasks for an HKM. In contrast to the 3-PRS mechanism, the 3-PUU mechanism doesn't require precise spherical joints, and its revolution joints are correspondingly unrestricted to the cone angle constraints of those spherical joints. Thus, it's easier and cheaper to develop a 3-PUU mechanism in practice, and it has the potential of offering better orientation capability.

Due to its special physical constraints, kinematics and dynamics analyses for the proposed 3-PUU parallel mechanism are more complicated than the current one. The geometrical constraints of this mechanism are obtained according to its special mechanism architecture and link structure. Then, the parasitic motion of the 3-PUU is derived and explicitly expressed by using the substitution method. Inverse kinematics analysis and forward kinematics analysis are, respectively, carried out with the vector loop method[1,2] and Newton iteration method,[1,2] both of which are classical methods of the field. In addition, the key issue for dynamics analysis is to establish an inverse dynamics model of the parallel mechanism, which can yield the required actuated force given a desired trajectory of the moving platform. The literature of dynamics analysis for PKMs reports various methods to formulate the inverse dynamic equations. These formulations include the Newton–Euler method,[24] Lagrange approach,[25] Kane's equations, [26] and The Principle of Virtual Work.[27] The dynamic model of the 3-PUU parallel mechanism in the present work is based on The Principle of Virtual Work, which is an energy-based formulation with relatively simple and compact symbolic description and can produce abundant analytical results.

The paper is organized as follows: Section 1 provides the introduction. In Section 2, a detailed description on 3-PUU architecture and its geometrical constraints is presented. In Section 3, based on the special geometrical constraints of the mechanism, its parasitic motions are derived and explicitly expressed; then, we solve the inverse kinematics problem (IKP) and forward kinematics problem (FKP) according to the parasitic motions results. Section 4 states the dynamics analysis of the proposed 3-PUU mechanism. Section 5 is the conclusion.

2. Architecture Description and Mobility Analysis

2.1. Architecture description and geometrical constraints

The CAD model of the proposed 3-PUU mechanism is presented in Fig. 1(a), where $O - xyz$ is the global coordinate frame, $A_1 - x_1y_1z_1$ is the local coordinate frame built on the P joint of limb 1. It is made up of a moving platform, three ground-fixed vertical columns and three identical limbs. The whole structure is cyclic symmetric around z-axis. Π_1 represents the vertical plane that linkage A_1B_1 currently belongs to. Figure 1(b) demonstrates the geometry model of limb 1. Each limb connects a fixed column to the mobile platform by one P joint followed by two U joints. A linear actuator drives each of the three P joints along EE', and the four revolute axes of the two U joints in limb 1 are DD', CC', BB' and AA'. When the linkage rotates about DD' with angle θ, the vertical plane Π_1 rotates correspondingly.

The main distinction between the 3-PUU mechanism illustrated in Fig. 1(a) and the 3-PUU proposed by Tsai[7,19,20] lies in their U joints. The U joints depicted in Fig. 1(b) satisfies the following physical constraints: The first revolute axis DD' is parallel to the moving direction of the P joints, i.e., EE'; the second revolute axis CC' is parallel to the third revolute axis BB', and they are perpendicular

https://doi.org/10.1017/S0263574716000692 Published online by Cambridge University Press

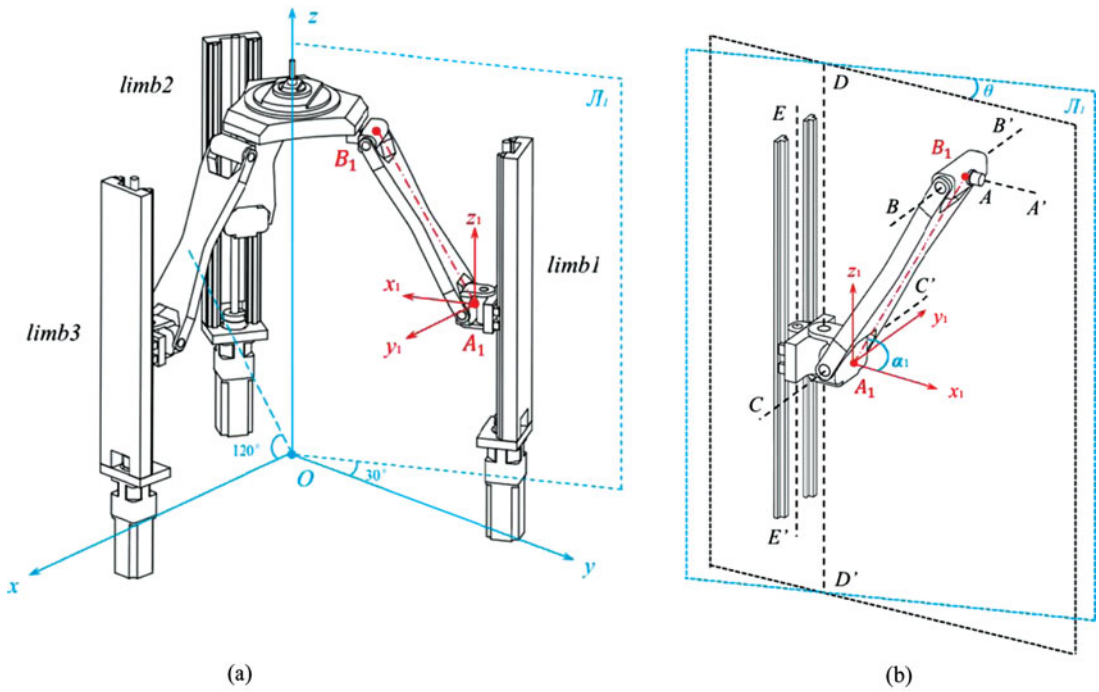

Fig. 1. CAD models of 3-PUU parallel kinematic mechanism. (a) CAD model of the 3-PUU mechanism. (b) CAD model of limb1.

to the first revolute axis $DD^{'}$ and the symmetric axis A_1B_1 of linkage 1 at the same time; the fourth revolute axis $AA^{'}$ is perpendicular to the third revolute axis $BB^{'}$. Nonetheless, in the limb of Tsai's 3-PUU mechanism, its two U joints are totally identical, i.e., its first revolute axis is parallel to its fourth revolute axis, and its second revolute axis is parallel to its third revolute axis. Such a minor difference in their U joints arrangement leads to a great gap between their DOFs' properties: The former one owns 2R1T DOFs and can be used as an orientation mechanism, whereas the latter one has three pure translational (3T) DOFs and should be utilized as a position mechanism.

The kinematic scheme of the proposed 3-PUU mechanism in an arbitrary configuration is depicted in Fig. 2(a), whose projection on the Oxy plane is shown in Fig. 2(b), and limb 1 and its own coordinate system $A_1 - x_1y_1z_1$ are shown in Fig. 2(c). For analysis, a moving coordinate frame $M - uvw$ is attached on the centered point M of the moving platform. In addition, three local coordinate systems $A_i - x_iy_iz_i$ are built and attached on their P joint, and their corresponding directions are illustrated in Fig. 2(a). R and r are, respectively, the radius of circles with centered point M and O; L is the length of linkage A_iB_i, h_i denotes the actuated height of three P joints. The architectural parameters of the 3-PUU parallel manipulator studied in this paper are set as follows: $R = 400$ mm, $r = 200$ mm and $L = 550$ mm. As Fig. 1(b) demonstrate, the local frame $A_i - x_iy_iz_i$ will rotate around A_iz_i when three actuated P joints moves, and the intersection angle between $A_i - x_iy_iz_i$ and $O - xyz$ around z-axis is θ_i, just like Fig. 2(b) illustrates.

Through observing the geometry structure of the 3-PUU mechanism illustrated in Fig. 1(a)–(c), we can identify the core geometrical constraints of the 3-PUU mechanism: Due to the inherent constraint of the second revolute joint CC', the motion of each limb is limited in its own plane Π_i, which is always vertical to the Oxy plane. Moreover, the plane Π_i could rotate around axis DD', where the first revolute joint exists. Thus, the motion of the whole mechanism can be projected to the Oxy plane as Fig. 2(b) depicts, where A_i^{Oxy}, B_i^{Oxy} and M^{Oxy} $(i = 1, 2, 3)$ denote the projection points of A_i, B_i and M on the Oxy plane, respectively; lines $A_i^{Oxy}B_i^{Oxy}$ $(i = 1, 2, 3)$ represents the projection of plane Π_i. Just like Fig. 1(b) presents, the third revolute joint BB' brings about the physical constraint that the fourth revolute axis AA' always stay in plane Π_i. In addition, because AA' passes through the

https://doi.org/10.1017/S0263574716000692 Published online by Cambridge University Press

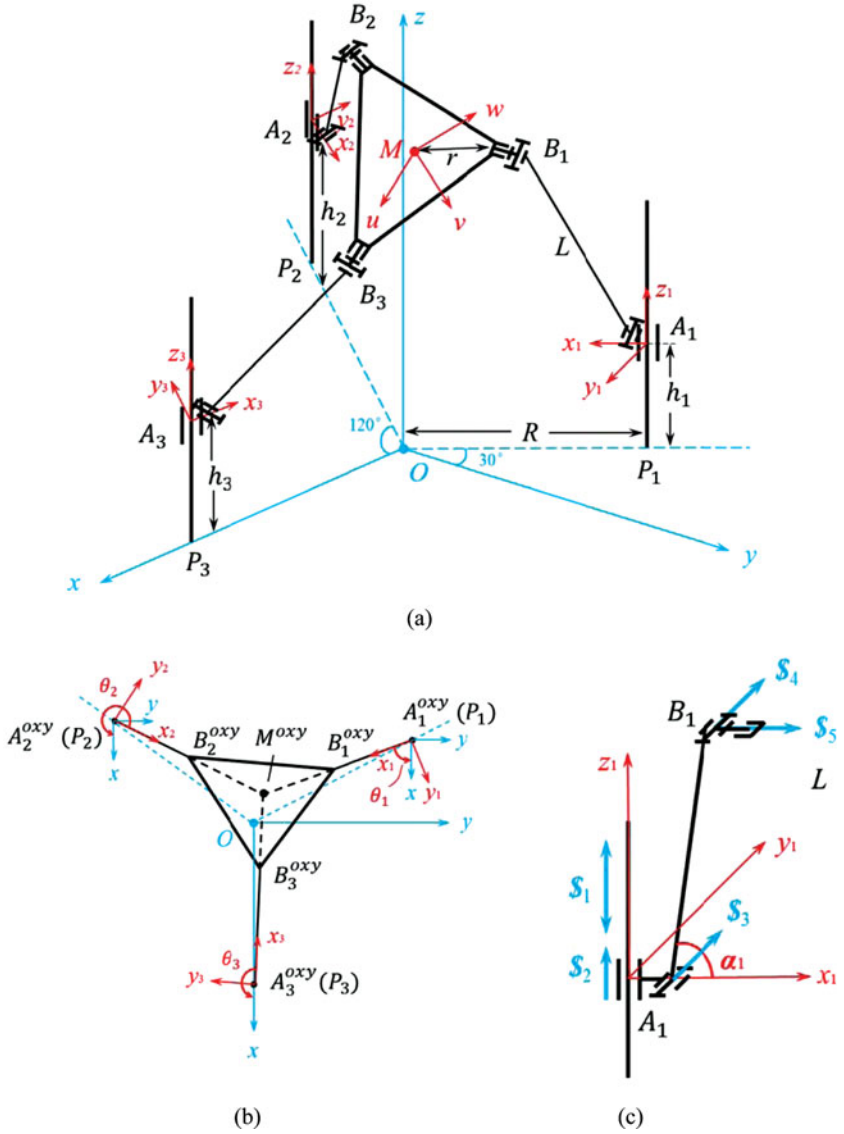

Fig. 2. Schematic representation of the 3-PUU PKM. (a) The 3-PUU PKM (b) Projection of 3-PUU mechanism on *Oxy* plane. (c) The sketch of limb1.

centered point of the moving platform M, each plane Π_i $(i = 1, 2, 3)$ includes M in it. Hence, as Fig. 2(b) illustrates, in the projection of the 3-PUU mechanism on the *Oxy* plane, $A_i^{Oxy}B_i^{Oxy}$ $(i = 1,\ 2,\ 3)$ perpetually intersect at M^{Oxy}. The above physical constraints are able to be described as follows:

$$\begin{cases} A_1^{oxy}B_1^{oxy} \cap A_2^{oxy}B_2^{oxy} = M^{oxy} \\ A_1^{oxy}B_1^{oxy} \cap A_3^{oxy}B_3^{oxy} = M^{oxy} \\ A_2^{oxy}B_2^{oxy} \cap A_3^{oxy}B_3^{oxy} = M^{oxy} \end{cases}, \tag{1}$$

which is the exclusive constraints the proposed 3-PUU satisfies.

2.2. Mobility analysis

We would like to apply the screw theory[28,29] to analyze the DOFs of the 3-PUU mechanism, this approach yields all mobility information for a PKM, e.g., the number, type and direction of its DOFs. Since the three limbs are identical, only one of them needs to be analyzed under its local frame. According to Fig. 2(c), we can obtain the twist screws of all five motion pairs in limb i $(i = 1,\ 2,\ 3)$

https://doi.org/10.1017/S0263574716000692 Published online by Cambridge University Press

as follows:

$$\begin{cases} \$_1 = (0,\ 0,\ 0;\ 0,\ 0,\ 1) \\ \$_2 = (0, 0,\ 1;\ 0,\ 0,\ 0) \\ \$_3 = (0,\ 1,\ 0;\ 0, 0, 0) \\ \$_4 = (0,\ 1,\ 0;\ -L\sin\alpha_i, 0,\ L\cos\alpha_i) \\ \$_5 = (1,\ 0,\ 0;\ 0, L\sin\alpha_i, 0) \end{cases}. \tag{2}$$

It's not difficult to work out the reciprocal screw of the above five screws under local frame $A_i - x_i y_i z_i$ as follows:

$$\$^r_{\text{limbi}-\text{local}} = (0,\ 1,\ 0;\ -L\sin\alpha_i,\ 0,\ 0). \tag{3}$$

Based on transformation approaches proposed in the literature,[30] we are able to transform $\$^r_{\text{limbi}-\text{local}}$ from local coordinate systems to the global coordinate system:

$$\begin{cases} \$^r_{\text{limb1}-\text{global}} = (\sin\theta_1,\ \cos\theta_1,\ 0; -h_1\cos\theta_1 - L\sin\alpha_1\cos\theta_1,\ h_1\sin\theta_1 + L\sin\alpha_1\sin\theta_1,\ -\frac{1}{2}R\cos\theta_1 - \frac{\sqrt{3}}{2}R\sin\theta_1) \\ \$^r_{\text{limb2}-\text{global}} = (\sin\theta_2,\ \cos\theta_2,\ 0; -h_2\cos\theta_2 - L\sin\alpha_2\cos\theta_2,\ h_2\sin\theta_2 + L\sin\alpha_2\sin\theta_2,\ -\frac{1}{2}R\cos\theta_2 + \frac{\sqrt{3}}{2}R\sin\theta_2) \cdot \\ \$^r_{\text{limb3}-\text{global}} = (\sin\theta_3,\ \cos\theta_3,\ 0; -h_3\cos\theta_3 - L\sin\alpha_3\cos\theta_3,\ h_3\sin\theta_3 + L\sin\alpha_3\sin\theta_3,\ R\cos\theta_3) \end{cases} \tag{4}$$

First of all, let's consider the simplest situation, i.e., the moving platform is horizontal, where three actuated heights of P joints satisfy $h_1 = h_2 = h_3 = h$, three inclined angles of linkages meet $\alpha_1 = \alpha_2 = \alpha_3 = \alpha$, and three included angles between $A_i - x_i y_i z_i$ $(i = 1, 2, 3)$ and $O - xyz$ around z-axis are $\theta_1 = \frac{\pi}{3},\ \theta_2 = -\frac{\pi}{3},\ \theta_3 = \pi$. Substituting $h_i,\ \alpha_i$ and θ_i into Eq. (4), we can get

$$\begin{cases} \$^r_{\text{limb1}-\text{global}} = \left(\frac{\sqrt{3}}{2},\ \frac{1}{2},\ 0; -\frac{1}{2}(h + L\sin\alpha), \frac{\sqrt{3}}{2}(h + L\sin\alpha),\ -R\right) \\ \$^r_{\text{limb2}-\text{global}} = \left(-\frac{\sqrt{3}}{2},\ \frac{1}{2},\ 0; -\frac{1}{2}(h + L\sin\alpha), -\frac{\sqrt{3}}{2}(h + L\sin\alpha),\ -R\right) \cdot \\ \$^r_{\text{limb3}-\text{global}} = (0,\ -1,\ 0; h + L\sin\alpha, 0,\ -R) \end{cases} \tag{5}$$

Therefore, the instantaneous motion screws set of the end-effector is equal to

$$\$_{\text{end}-\text{effector}} = (\text{U}^3_{i=1}\$^r_{\text{limbi}-\text{global}})^r = \begin{cases} (0,\ 0,\ 0; 0,\ 0,\ 1) & (a) \\ (1,\ 0,\ 0; 0,\ h + L\sin\alpha,\ 0) & (b) \\ (0,\ 1,\ 0; -h - L\sin\alpha,\ 0, 0) & (c) \end{cases}, \tag{6}$$

wherein (a) denotes a translation DOF along z direction, (b) denotes a revolution DOF around x-axis with parasitic motion along y direction and (c) denotes a revolution DOF around y-axis with parasitic motion along x direction.

The mobility analysis of 3-PUU in an arbitrary configuration is also conducted. Since it's difficult to analytically express the reciprocal screws of $\$^r_{\text{limbi}-\text{global}},\ (i = 1,\ 2,\ 3)$ in Eq. (4), i.e., $\$ = (\text{U}^3_{i=1}\$^r_{\text{limbi}-\text{global}})^r$, a Matlab program for realizing following functions is coded and implemented:

(i) Transform the issue of solving the reciprocal screws of $\$^r_{\text{limbi}-\text{global}},\ (i = 1,\ 2,\ 3)$ to the problem of solving an underdetermined system of equations, and then calculate $\$ with corresponding algorithms in the latter field.
(ii) Produce the reduced row echelon form of the determinant of $\$, and the rank of it is equal to the DOFs number of this mechanism.
(iii) Judge the DOFs' type and direction based on the reduced row echelon form in ii.

https://doi.org/10.1017/S0263574716000692 Published online by Cambridge University Press

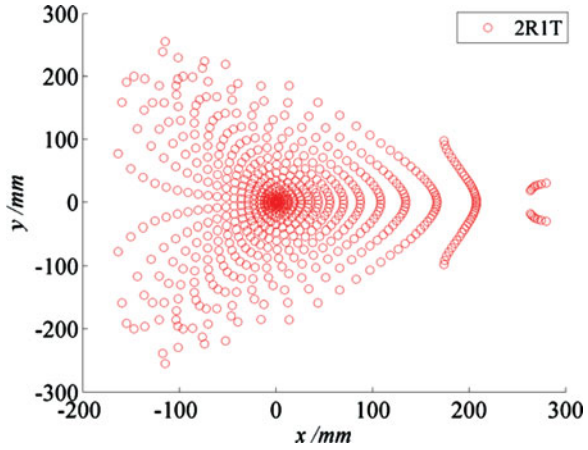

Fig. 3. General DOF properties of the 3-PUU mechanisms over its reachable workspace.

Due to the fact that $\$_a = (0,\ 0,\ 0;\ 0,\ 0,\ 1)$ is always reciprocal with $\$^r_{\text{limbi}-\text{global}},\ (i = 1,\ 2\ ,3)$ in Eq. (4), which means an independent translational DOF along z direction, we just need ascertain the other two DOFs' properties at an given z displacement. Let the X and Y rotational angles vary from $-\frac{\pi}{2}$ to $\frac{\pi}{2}$, and the input actuated displacement ranges within $[-300\text{ mm},\ 300\text{ mm}]$. The DOFs properties of the 3-PUU mechanism over its reachable workspace are illustrated with Fig. 3, where 2R1T denotes a rotational DOF around x-axis, a rotational DOF around y-axis, and a translational DOF along z direction. Obviously, although the configuration varies, the DOF properties remain unchanged over the workspace. Hence, from the perspective of mobility, the 3-PUU mechanism generally meets the requirement of a machine tool head.

3. Kinematics Analysis

Kinematics analysis includes inverse kinematics analysis and forward kinematic analysis. The inverse position kinematics solves the input actuated variables $\boldsymbol{h} = [h_1, h_2, h_3]^T$ from a given output position and orientation, which is $\boldsymbol{x} = [M_z, \psi, \theta]^T$ for the ZXY Euler angle convention. In contrast, the forward position kinematics solves the output position and orientation $\boldsymbol{x}$ of the moving platform with given actuated input $\boldsymbol{h}$. Inverse kinematics analysis is the base for all further study of a mechanism.

3.1. Parasitic motion

For those mechanisms with parasitic motions, the key step for their inverse kinematics analysis is to carry out the expression of its parasitic motion according to the geometrical constraints.

Equation (1) can be expressed as

$$\begin{cases} A_1^{oxy} B_1^{oxy} // B_1^{oxy} M^{oxy} \\ A_2^{oxy} B_2^{oxy} // B_2^{oxy} M^{oxy} \\ A_3^{oxy} B_3^{oxy} // B_3^{oxy} M^{oxy} \end{cases}. \tag{7}$$

Assuming that the x and y coordinates of point X_i^{oxy} are expressed as X_i^{oxy} (1) and X_i^{oxy} (2), Eq. (7) can be transformed to algebraic form:

$$\begin{cases} \left(A_1^{oxy}(2) - B_1^{oxy}(2)\right)\left(B_1^{oxy}(1) - M^{oxy}(1)\right) = \left(A_1^{oxy}(1) - B_1^{oxy}(1)\right)\left(B_1^{oxy}(2) - M^{oxy}(2)\right) \\ \left(A_2^{oxy}(2) - B_2^{oxy}(2)\right)\left(B_2^{oxy}(1) - M^{oxy}(1)\right) = \left(A_2^{oxy}(1) - B_2^{oxy}(1)\right)\left(B_2^{oxy}(2) - M^{oxy}(2)\right) \\ \left(A_3^{oxy}(2) - B_3^{oxy}(2)\right)\left(B_3^{oxy}(1) - M^{oxy}(1)\right) = \left(A_3^{oxy}(1) - B_3^{oxy}(1)\right)\left(B_3^{oxy}(2) - M^{oxy}(2)\right) \end{cases}. \tag{8}$$

https://doi.org/10.1017/S0263574716000692 Published online by Cambridge University Press

According to Fig. 2(b),

$$\begin{cases} P_i(1) = A_i^{oxy}(1) = R\cos\left(\frac{2i}{3}\pi\right) \\ P_i(2) = A_i^{oxy}(2) = R\sin\left(\frac{2i}{3}\pi\right), \quad i = 1,\ 2,\ 3. \\ P_i(3) = A_i^{oxy}(3) = 0 \end{cases} \tag{9}$$

As depicted in Fig. 2(a), the position vector of points A_i and points B_i with respect to frame O and frame M can be written as $\boldsymbol{A}_i^O$ and $\boldsymbol{B}_i^M$, respectively, where a superscript indicates the coordinate frame with respect to which a vector is defined. For brevity, the superscript will always be omitted whenever the coordinate frame is the fixed frame, e.g., $\boldsymbol{B}_i^O = \boldsymbol{B_i}$. Thus, there is

$$\boldsymbol{B}_i = \boldsymbol{M} + \boldsymbol{R}_M^O(\theta, \psi, \phi) \cdot \boldsymbol{B_i^M}, \quad i = 1,\ 2,\ 3, \tag{10}$$

where the rotation matrix between the moving frame and the fixed frame

$$\begin{aligned} \boldsymbol{R}_M^O(\theta, \psi, \phi) &= \boldsymbol{R}_y(\theta)\,\boldsymbol{R}_x(\psi)\,\boldsymbol{R}_z(\phi) \\ &= \begin{bmatrix} c\theta c\phi + s\psi s\theta s\phi & -c\theta s\phi + s\psi s\theta c\phi & c\psi s\theta \\ c\psi s\phi & c\psi c\phi & -s\psi \\ -s\theta c\phi + s\psi c\theta s\phi & s\theta s\phi + s\psi c\theta c\phi & c\psi c\theta \end{bmatrix}, \end{aligned} \tag{11}$$

and

$$\begin{cases} \boldsymbol{B}_i^M(1) = r\ \cos\left(\frac{2i}{3}\pi\right) \\ \boldsymbol{B}_i^M(2) = r\ \sin\left(\frac{2i}{3}\pi\right), \quad i = 1,\ 2,\ 3. \\ \boldsymbol{B}_i^M(3) = 0 \end{cases} \tag{12}$$

For $i = 1$, substituting Eqs. (11) and (12) into Eq. (10), it yields

$$\begin{cases} B_1^{oxy}(1) = M(1) + (c\theta c\phi + s\psi s\theta s\phi) r\cos\left(\frac{2}{3}\pi\right) + (-c\theta s\phi + s\psi s\theta c\phi) r\sin\left(\frac{2}{3}\pi\right) \\ B_1^{oxy}(2) = M(2) + (c\psi s\phi) r\cos\left(\frac{2}{3}\pi\right) + (c\psi c\phi) r\sin\left(\frac{2}{3}\pi\right). \end{cases} \tag{13}$$

Let

$$\begin{cases} M_1 = (c\theta c\phi + s\psi s\theta s\phi) r\cos\left(\frac{2}{3}\pi\right) + (-c\theta s\phi + s\psi s\theta c\phi) r\sin\left(\frac{2}{3}\pi\right) \\ N_1 = (c\psi s\phi) r\cos\left(\frac{2}{3}\pi\right) + (c\psi c\phi) r\sin\left(\frac{2}{3}\pi\right) \end{cases}, \tag{14}$$

and then substituting Eqs. (14) and (13) into Eq. (8), we get

$$\left(A_1^{oxy}(2) - M(2) - N_1\right) M_1 = \left(A_1^{oxy}(1) - M(1) - M_1\right) N_1,$$

which can be simplified further as

$$\left(A_1^{oxy}(2) - M(2)\right) M_1 = \left(A_1^{oxy}(1) - M(1)\right) N_1. \tag{15a}$$

A similar process can also be executed for A_2^{oxy}, A_3^{oxy}, B_2^{oxy} and B_3^{oxy}, and yields

$$\left(A_2^{oxy}(2) - M(2)\right) M_2 = \left(A_2^{oxy}(1) - M(1)\right) N_2, \tag{15b}$$

$$\left(A_3^{oxy}(2) - M(2)\right) M_3 = \left(A_3^{oxy}(1) - M(1)\right) N_3, \tag{15c}$$

https://doi.org/10.1017/S0263574716000692 Published online by Cambridge University Press

where

$$\begin{cases} M_2 = (c\theta c\phi + s\psi s\theta s\phi)\, r\, \cos\left(\frac{4}{3}\pi\right) + (-c\theta s\phi + s\psi s\theta c\phi)\, r\, \sin\left(\frac{4}{3}\pi\right) \\ N_2 = (c\psi s\phi)\, r\, \cos\left(\frac{4}{3}\pi\right) + (c\psi c\phi)\, r\, \sin\left(\frac{4}{3}\pi\right) \\ M_3 = (c\theta c\phi + s\psi s\theta s\phi)\, r \\ N_3 = (c\psi s\phi)\, r \end{cases}. \tag{16}$$

Let

$$\begin{cases} S = c\theta c\phi + s\psi s\theta s\phi \\ T = -c\theta s\phi + s\psi s\theta c\phi \\ U = c\psi s\phi \\ V = c\psi c\phi \end{cases}, \tag{17}$$

and then Eqs. (14) and (16) can be transformed to

$$\begin{cases} M_1 = S \cdot r\, \cos\left(\frac{2}{3}\pi\right) + T \cdot r\, \sin\left(\frac{2}{3}\pi\right) \\ N_1 = U \cdot r\, \cos\left(\frac{2}{3}\pi\right) + V \cdot r\, \sin\left(\frac{2}{3}\pi\right) \\ M_2 = S \cdot r\, \cos\left(\frac{4}{3}\pi\right) + T \cdot r\, \sin\left(\frac{4}{3}\pi\right) \\ N_2 = U \cdot r\, \cos\left(\frac{4}{3}\pi\right) + V \cdot r\, \sin\left(\frac{4}{3}\pi\right) \\ M_3 = S \cdot r \\ N_3 = U \cdot r \end{cases}. \tag{18}$$

Thus, Eqs. (15a)–(15c) can be rewritten as

$$\begin{aligned} &\left(A_1^{oxy}(2) - M(2)\right)\left(S \cdot r\, \cos\left(\tfrac{2}{3}\pi\right) + T \cdot r\, \sin\left(\tfrac{2}{3}\pi\right)\right) \\ &\quad = \left(A_1^{oxy}(1) - M(1)\right)\left(U \cdot r\, \cos\left(\tfrac{2}{3}\pi\right) + V \cdot r\, \sin\left(\tfrac{2}{3}\pi\right)\right) \end{aligned} \tag{19a}$$

$$\begin{aligned} &\left(A_2^{oxy}(2) - M(2)\right)\left(S \cdot r \cos\left(\tfrac{4}{3}\pi\right) + T \cdot r\, \sin\left(\tfrac{4}{3}\pi\right)\right) \\ &\quad = \left(A_2^{oxy}(1) - M(1)\right)\left(U \cdot r\, \cos\left(\tfrac{4}{3}\pi\right) + V \cdot r\, \sin\left(\tfrac{4}{3}\pi\right)\right) \end{aligned} \tag{19b}$$

$$\left(A_3^{oxy}(2) - M(2)\right) S \cdot r = \left(A_3^{oxy}(1) - M(1)\right) U \cdot r. \tag{19c}$$

We take $M(1)$ and $M(2)$ as two unknown variables here, they can be analytically expressed by considering the formulas (19a) and (19b):

$$\begin{cases} M(1) = \dfrac{(I - H) \cdot T \cdot \sin\left(\frac{2}{3}\pi\right) + (J - K) \cdot S \cdot \cos\left(\frac{2}{3}\pi\right)}{2r \cdot (U \cdot T - V \cdot S) \cdot \cos\left(\frac{2}{3}\pi\right) \sin\left(\frac{2}{3}\pi\right)} \\ M(2) = \dfrac{(H - I) \cdot V \cdot \sin\left(\frac{2}{3}\pi\right) + (K - J) \cdot U \cdot \cos\left(\frac{2}{3}\pi\right)}{2r \cdot (V \cdot S - U \cdot T) \cdot \cos\left(\frac{2}{3}\pi\right) \sin\left(\frac{2}{3}\pi\right)} \end{cases}, \tag{20}$$

where

$$\begin{cases} H = A_1^{oxy}(2)\, M_1 + A_2^{oxy}(2)\, M_2 \\ I = A_1^{oxy}(1)\, N_1 + A_2^{oxy}(1)\, N_2 \\ J = A_1^{oxy}(2)\, M_1 - A_2^{oxy}(2)\, M_2 \\ K = A_1^{oxy}(1)\, N_1 - A_2^{oxy}(1)\, N_2 \end{cases}. \tag{21}$$

https://doi.org/10.1017/S0263574716000692 Published online by Cambridge University Press

Equation (20) is the analytical expression of two translation parasitic motions, which is dependent on the unknown variable ϕ . Substituting Eq. (9) into Eq. (19c), we achieve

$$(0 - M(2)) \cdot S = (R - M(1)) \cdot U. \tag{22}$$

We further substitute Eq. (20) into Eq. (22), and get

$$\frac{\left((I-H)\cdot T\cdot \sin\left(\frac{2}{3}\pi\right)+(J-K)\cdot S\cdot \cos\left(\frac{2}{3}\pi\right)\right)\cdot U+\left((H-I)\cdot V\cdot \sin\left(\frac{2}{3}\pi\right)+(K-J)\cdot U\cdot \cos\left(\frac{2}{3}\pi\right)\right)\cdot S}{2r\cdot(U\cdot T-V\cdot S)\cdot \cos\left(\frac{2}{3}\pi\right)\sin\left(\frac{2}{3}\pi\right)} = R\cdot U,$$

which can also be expressed as

$$\frac{(I-H)\cdot \sin\left(\frac{2}{3}\pi\right)\cdot(T\cdot U-V\cdot S)}{2r\cdot(U\cdot T-V\cdot S)\cdot \cos\left(\frac{2}{3}\pi\right)\sin\left(\frac{2}{3}\pi\right)} = R\cdot U,$$

which can be further simplified as

$$\frac{I-H}{2r\cdot \cos\left(\frac{2}{3}\pi\right)} = R\cdot U,$$

that is,

$$I - H = 2R\cdot r\cdot U\cdot \cos\left(\frac{2}{3}\pi\right). \tag{23}$$

Substituting Eqs. (9), (18) and (21) into Eq. (23), we obtain the following results after finishing:

$$2R\cdot r\cdot\left(U\cdot\cos^2\left(\frac{2\pi}{3}\right)-T\cdot\sin^2\left(\frac{2\pi}{3}\right)\right) = 2R\cdot r\cdot U\cdot \cos\left(\frac{2}{3}\pi\right),$$

which can be simplified as

$$\frac{1}{4}U - \frac{3}{4}T = -\frac{1}{2}U,$$

that is,

$$U = T. \tag{24}$$

Considering Eq. (17), (24) can be expressed as

$$c\psi s\phi = -c\theta s\phi + s\psi s\theta c\phi, \tag{25}$$

which combined with $s^2\phi + c^2\phi = 1$ can be used to solve ϕ :

$$\phi = \operatorname{asin}\left(\frac{\sin\psi\,\sin\theta}{\cos\psi\,\cos\theta+1}\right). \tag{26}$$

Since parasitic motions $M(1)$ and $M(2)$ in Eq. (20) depend on ϕ, now they can be calculated by substituting Eq. (26) into Eq. (20). Up to now, we have completed the explicit expression of all three parasitic motion parameters $(M_x,\ M_y,\ \phi)$. Given the orientation range $\psi,\ \theta \in [-\frac{\pi}{3},\ \frac{\pi}{3}]$, and then the parasitic motion of 3-PUU mechanism can be achieved according to Eqs. (20) and (26). The mapping relationships between $M_x,\ M_y,\ \phi$ and $\psi,\ \theta$ are, respectively, presented in Fig. 4 (a)–(c), all of which are saddle surfaces. Both the maximum and the minimum magnitudes of all three parasitic motions happen at four end-point $(-\frac{\pi}{3},\ -\frac{\pi}{3})$, $(-\frac{\pi}{3},\ \frac{\pi}{3})$, $(\frac{\pi}{3},\ -\frac{\pi}{3})$ and $(\frac{\pi}{3},\ \frac{\pi}{3})$, which represent four extreme configurations, the mechanism reaches at four different directions. Obviously, the higher ψ and θ the greater parasitic motion.

https://doi.org/10.1017/S0263574716000692 Published online by Cambridge University Press

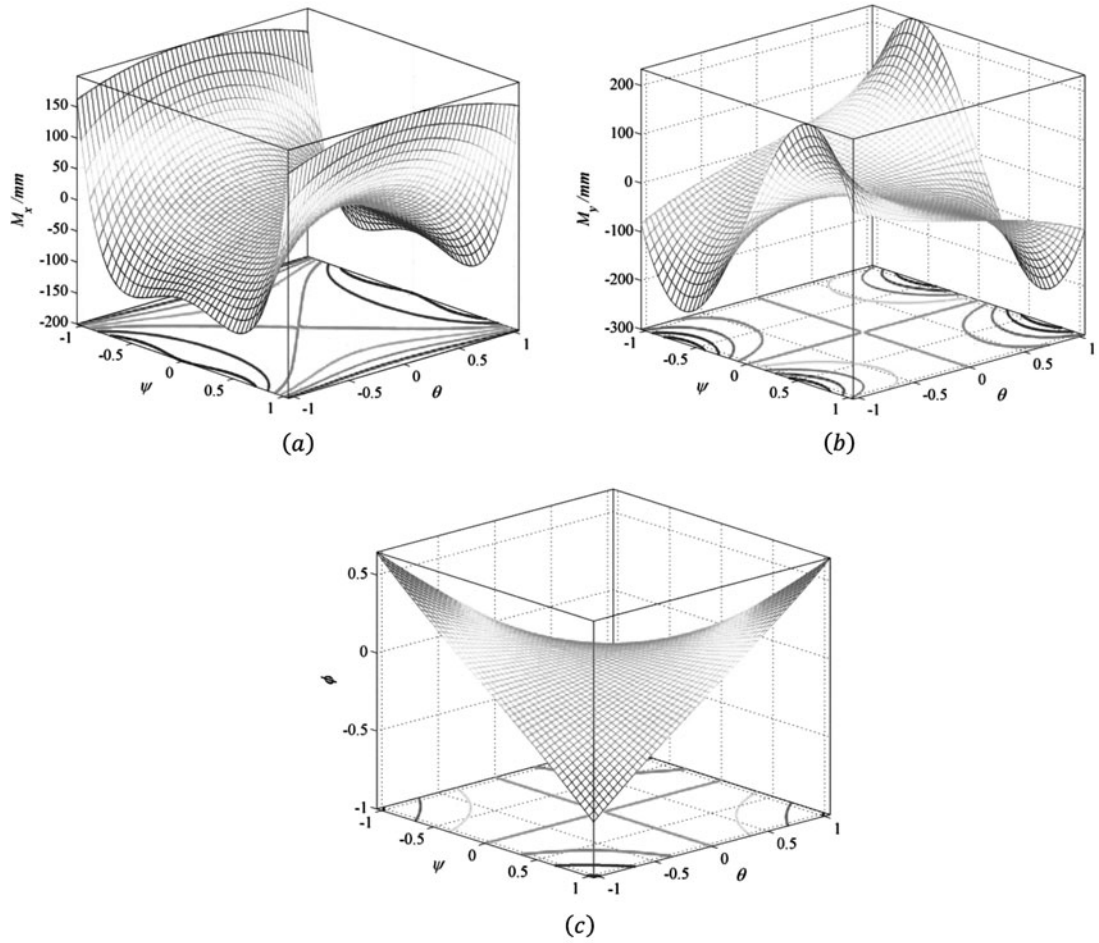

Fig. 4. The relationship between parasitic motions M_x, M_y, Φ and ψ, θ. (a) M_x. (b) M_y. (c) Φ.

3.2. Inverse kinematics problem

Referring to Fig. 2(a), the position vector pointing from O to B_i can be written in the vector loop form:

$$\boldsymbol{B}_i = \boldsymbol{M} + \boldsymbol{b}_i = \boldsymbol{P_i} + h_i \boldsymbol{e}_z + L\boldsymbol{L}_{ie}, \quad i = 1,\ 2,\ 3, \tag{27}$$

where $\boldsymbol{b}_i = \boldsymbol{R}_M^O \cdot \boldsymbol{B}_i^M$, $\boldsymbol{P_i}$ is expressed in Eq. (9), $\boldsymbol{e}_z = [0\ 0\ 1]^T$, $\boldsymbol{L}_{ie}$ is the unit vector directing along $\overrightarrow{A_i B_i}$, for $i = 1, 2, 3$.

Equation (27) can be transformed to algebraic form:

$$|\boldsymbol{A_i} - \boldsymbol{B}_i| = |\boldsymbol{P_i} + h_i \boldsymbol{e}_z - \boldsymbol{B}_i| = L, \quad i = 1,\ 2,\ 3. \tag{28}$$

Thus, $\boldsymbol{h} = [h_1, h_2, h_3]$ can be resolved from Eq. (28) as follows:

$$h_i = B_i\,(3) - \sqrt{L^2 - (P_i\,(1) - B_i\,(1))^2 - (P_i\,(2) - B_i\,(2))^2}, \quad i = 1,\ 2,\ 3, \tag{29}$$

where $P_i(j)$ and $B_i(j)$, respectively, denote the jth components of P_i and B_i in Eqs. (9) and (10).

https://doi.org/10.1017/S0263574716000692 Published online by Cambridge University Press

In addition, according to the geometry relationship illustrated in Fig. 2(b), α_i and θ_i described in Figs. 1(b) and 2(b) can be expressed as follows:

$$\begin{cases} \alpha_i = \text{acos}\left(\dfrac{\sqrt{(B_i(1) - A_i(1))^2 + (B_i(2) - A_i(2))^2}}{L}\right) \\ \theta_i = \text{atan}\left(\dfrac{B_i(2) - A_i(2)}{B_i(1) - A_i(1)}\right) \end{cases}, \quad i = 1,\ 2,\ 3. \tag{30}$$

3.3. Forward kinematics problem

The Jacobian matrix is the key for forward position kinematics analysis, and it represents the mapping relationship between the output velocity and the input velocity. The three independent output variables are $\dot{\boldsymbol{x}} = [\dot{M}_z, \dot{\psi}, \dot{\theta}]^T$.

Differentiating both sides of Eq. (27) with respect to time yields

$$\boldsymbol{v}_M + \boldsymbol{\omega}_M \times \boldsymbol{b}_i = \dot{h}_i \boldsymbol{e}_z + L\boldsymbol{\omega}_i \times \boldsymbol{L}_{ie}, \quad i = 1,\ 2,\ 3, \tag{31}$$

where $\boldsymbol{v}_M = [\,\dot{p}_x\ \dot{p}_y\ \dot{p}_z\,]^T$ and $\boldsymbol{\omega}_M = [\dot{\psi}\ \dot{\theta}\ \dot{\phi}]^T$ denote the spatial linear velocity and angular velocity of the moving platform, respectively, $\dot{h}_i$ represents the velocity of the ith prismatic joint, and $\boldsymbol{\omega}_i$ represents the spatial angular velocity of link A_iB_i.

To eliminate the passive variable $\boldsymbol{\omega}_i$, we dot-multiply both sides of Eq. (31) with $\boldsymbol{L}_{ie}$, which produces

$$\boldsymbol{L}_{ie} \cdot \boldsymbol{v}_M + \boldsymbol{L}_{ie} \cdot \boldsymbol{\omega}_M \times b_i = \dot{h}_i \boldsymbol{L}_{ie} \cdot \boldsymbol{e}_z, \quad i = 1,\ 2,\ 3. \tag{32}$$

Based on vector geometry knowledge in mathematics, it's easy to rewrite Eq. (32) as

$$\boldsymbol{L}_{ie} \cdot \boldsymbol{v}_M + (\boldsymbol{b}_i \times \boldsymbol{L}_{ie}) \cdot \boldsymbol{\omega}_M = \dot{h}_i \boldsymbol{L}_{ie} \cdot \boldsymbol{e}_z, \quad i = 1,\ 2,\ 3. \tag{33}$$

Let $\dot{\boldsymbol{X}} = [\boldsymbol{v}_M\ \boldsymbol{\omega}_M]^T$ and $\dot{\boldsymbol{h}} = [\dot{h}_1, \dot{h}_2, \dot{h}_3]^T$ be the generalized velocities of the moving platform and the actuated prismatic joints. Then, an equivalent matrix form of Eq. (33) can be obtained as

$$\boldsymbol{J}_x \cdot \dot{\boldsymbol{X}} = \boldsymbol{J}_h \cdot \dot{\boldsymbol{h}}, \tag{34}$$

where

$$\boldsymbol{J}_x = \begin{bmatrix} \boldsymbol{L}_{1e}^T & (\boldsymbol{b}_1 \times \boldsymbol{L}_{1e})^T \\ \boldsymbol{L}_{2e}^T & (\boldsymbol{b}_2 \times \boldsymbol{L}_{2e})^T \\ \boldsymbol{L}_{3e}^T & (\boldsymbol{b}_3 \times \boldsymbol{L}_{3e})^T \end{bmatrix}, \tag{35}$$

and

$$\boldsymbol{J}_h = \begin{bmatrix} \boldsymbol{L}_{1e} \cdot \boldsymbol{e}_z & 0 & 0 \\ 0 & \boldsymbol{L}_{2e} \cdot \boldsymbol{e}_z & 0 \\ 0 & 0 & \boldsymbol{L}_{3e} \cdot \boldsymbol{e}_z \end{bmatrix}, \tag{36}$$

when the manipulator is away from singularities, we have

$$\dot{\boldsymbol{h}} = \boldsymbol{J}_a \cdot \dot{\boldsymbol{X}}, \tag{37}$$

where $\boldsymbol{J}_a = \boldsymbol{J}_h^{-1} \cdot \boldsymbol{J}_x$ is a 3×6 matrix, and Eq. (37) represents the inverse velocity kinematics solution for 3-PUU PKM.

As we mentioned before, there are only three independent variables in $\dot{\boldsymbol{X}}$, namely, $\dot{\boldsymbol{x}} = [\dot{M}_z, \dot{\psi}, \dot{\theta}]^T$. And when the manipulator's configuration is away from singularity, we can transform $\dot{\boldsymbol{X}}$ to $\dot{\boldsymbol{x}}$, with

https://doi.org/10.1017/S0263574716000692 Published online by Cambridge University Press

following formula:

$$\dot{\boldsymbol{X}} = \boldsymbol{J}_r \cdot \dot{\boldsymbol{x}}, \tag{38}$$

where

$$\boldsymbol{J}_r = \begin{bmatrix} \dfrac{\partial M_x}{\partial M_z} & \dfrac{\partial M_x}{\partial \psi} & \dfrac{\partial M_x}{\partial \theta} \\ \dfrac{\partial M_y}{\partial M_z} & \dfrac{\partial M_y}{\partial \psi} & \dfrac{\partial M_y}{\partial \theta} \\ 1 & 0 & 0 \\ 0 & 1 & 0 \\ 0 & 0 & 1 \\ \dfrac{\partial \phi}{\partial M_z} & \dfrac{\partial \phi}{\partial \psi} & \dfrac{\partial \phi}{\partial \theta} \end{bmatrix}, \tag{39}$$

relative partial differentials in $\boldsymbol{J}_r$ can be deduced from Eqs. (20) and (26).

According to Eqs. (37) and (38), we gain

$$\dot{\boldsymbol{h}} = \boldsymbol{J} \cdot \dot{\boldsymbol{x}}, \tag{40}$$

wherein $\boldsymbol{J}$ is the 3×3 Jacobian matrix reflecting the relationship between input and output velocities of a 3-PUU PKM, and it can be written as

$$\boldsymbol{J} = \boldsymbol{J}_a \cdot \boldsymbol{J}_r. \tag{41}$$

Like most of the research in this field, the classical Newton iterative method is adopted here. The mathematical expression of the PKM system is

$$f(\boldsymbol{x}) = \boldsymbol{h}(\boldsymbol{x}) - \boldsymbol{h}_{\text{given}} = 0, \tag{42}$$

where $\boldsymbol{x} = [M_z, \psi, \theta]^T$, $\boldsymbol{h}(\boldsymbol{x})$ is the input referring to $\boldsymbol{x}$ and $\boldsymbol{h}_{\text{given}}$ is the required actuated inputs given in advance.

Let $\boldsymbol{x}^n = [x_1^n, x_2^n, x_3^n]$, and then the Newton iterative process is given as

$$\boldsymbol{x}^{k+1} = \boldsymbol{x}^k - \left[\frac{\partial f\left(\boldsymbol{x}^k\right)}{\partial \boldsymbol{x}}\right]^{-1} f\left(\boldsymbol{x}^k\right). \tag{43}$$

It is easy to know that $\frac{\partial f(\boldsymbol{x}^k)}{\partial \boldsymbol{x}} = \boldsymbol{J}(\boldsymbol{x}^k)$. Thus, Eq. (43) can be rewritten as

$$\boldsymbol{x}^{k+1} = \boldsymbol{x}^k - \left[\boldsymbol{J}\left(\boldsymbol{x}^k\right)\right]^{-1}\left[\boldsymbol{h}\left(\boldsymbol{x}^k\right) - \boldsymbol{h}_{\text{given}}\right]. \tag{44}$$

The iteration can be start with an initial output $\boldsymbol{x}^0$, and end when error $= \max(|\boldsymbol{h}(\boldsymbol{x}) - \boldsymbol{h}_{\text{given}}|) \leq \varepsilon$, where $\varepsilon = 10^{-3}$ mm is a specified tolerance.

4. Inverse Dynamics Analysis

Inverse dynamics solve the input actuated forces $\boldsymbol{f} = [f_1, f_2, f_3]^T$ from a given motion path of the moving platform, which can usually be expressed as the function of three output variables and time. The inverse position, velocity and acceleration kinematics are the bases for inverse dynamics analysis. Generally, designers of a mechanism hope to reduce its actuated forces as much as possible, which means that motors with lower performance level are enough.

https://doi.org/10.1017/S0263574716000692 Published online by Cambridge University Press

4.1. Dynamics parameters

The masses of the moving platform, the slider and the links of the 3-PUU PKM shown in Fig. 1 are $m_p = 1.0$ kg, $m_s = 0.2$ kg and $m_l = 0.2$ kg, respectively. For simplification,[9] the rotational inertias of three links are neglected. The mass of every link is divided into two portions, and imposed on their two extremities, i.e., half to the slider and half to the moving platform. Thus, the equivalent mass of the slider and the moving platform respectively are

$$\hat{m}_s = m_s + 0.5m_l \text{ and } \hat{m}_p = m_p + 0.5m_l.$$

The inertial matrix of the moving platform with respect to the fixed frame can be expressed as

$$\boldsymbol{I}_p = R_P^O \boldsymbol{I'}_P \left(R_P^O\right)^T, \tag{45}$$

where I'_P represents the inertial matrix of the moving platform under frame M, and can be written as

$$\boldsymbol{I'}_P = \hat{m}_p \begin{bmatrix} r^2/4 & 0 & 0 \\ 0 & r^2/4 & 0 \\ 0 & 0 & r^2/4 \end{bmatrix}.$$

4.2. T-T angle convention

Bonev[31] previously investigated the relationship between different kinds of Euler angles and the Tilt-and-Torsion (T-T) angles in detail. Bonev pointed out that the 3-[PP]S mechanism is a class of 3-DOF spatial parallel mechanism with zero-Torsion, i.e., the orientation of its moving platform can be described with only two variables, the azimuth angle α and the tilt angle β . Thus, it is usually more concise and more efficient to utilize the T-T angle, rather than the widely-used Euler angles, to solve kinematics and dynamics problems of a 3-[PP]S mechanism. Thus, the T-T angle convention is introduced here. The rotation matrix for the T-T angle convention is given as

$$\begin{aligned} {}^{TT}\boldsymbol{R}_P^O(\alpha, \beta, 0) &= \boldsymbol{R}_z(\alpha)\, \boldsymbol{R}_y(\beta)\, \boldsymbol{R}_z(-\alpha)\, \boldsymbol{R}_z(0) \\ &= \begin{bmatrix} c^2\alpha c\beta + s^2\alpha & s\alpha c\alpha\,(c\beta - 1) & c\alpha s\beta \\ s\alpha c\alpha\,(c\beta - 1) & s^2\alpha c\beta + c^2\alpha & s\alpha s\beta \\ -c\alpha s\beta & -s\alpha s\beta & c\beta \end{bmatrix}. \end{aligned} \tag{46}$$

According to Eqs. (11) and (46), T-T angles can be transformed to ZXY Euler angles via the following formulas:

$$\begin{cases} \psi = a\sin\,(-s\alpha s\beta) \\ \theta = a\sin\left(\dfrac{c\alpha s\beta}{c\psi}\right) \\ \phi = a\tan\left(\dfrac{s\psi s\theta}{c\psi + c\theta}\right) \end{cases}. \tag{47}$$

Through computation, ϕ solved from parasitic motion Eq. (26) and ϕ obtained from transformation Eq. (47) can be treated as the same one. Thus, we can come to the conclusion that the 3-PUU mechanism proposed in this paper is also a mechanism with zero-torsion, and it can be analyzed with the T-T angle.

The geometrical effects of $\dot{\boldsymbol{x}}_{tt} = [\dot{M}_z, \dot{\alpha}, \dot{\beta}]^T$ and $\dot{\boldsymbol{x}} = [\dot{M}_z, \dot{\psi}, \dot{\theta}]^T$ on 3-PUU PKM's configuration are the same, corresponding mapping formula between them can be expressed as

$$\dot{\boldsymbol{x}} = \boldsymbol{J}_t \cdot \dot{\boldsymbol{x}}_{tt}, \tag{48}$$

https://doi.org/10.1017/S0263574716000692 Published online by Cambridge University Press

where

$$\boldsymbol{J}_t = \begin{bmatrix} \frac{\partial M_z}{\partial M_z} & \frac{\partial M_z}{\partial \alpha} & \frac{\partial M_z}{\partial \beta} \\ \frac{\partial \psi}{\partial M_z} & \frac{\partial \psi}{\partial \alpha} & \frac{\partial \psi}{\partial \beta} \\ \frac{\partial \theta}{\partial M_z} & \frac{\partial \theta}{\partial \alpha} & \frac{\partial \theta}{\partial \beta} \end{bmatrix} = \begin{bmatrix} 1 & 0 & 0 \\ 0 & \frac{\partial \psi}{\partial \alpha} & \frac{\partial \psi}{\partial \beta} \\ 0 & \frac{\partial \theta}{\partial \alpha} & \frac{\partial \theta}{\partial \beta} \end{bmatrix}, \tag{49}$$

the partial differentials between $\psi,\ \theta$ and $\alpha,\ \beta$ can be obtained from Eq. (47).

In view of Eqs. (40) and (48), we can get

$$\dot{\boldsymbol{h}} = \boldsymbol{J}_{tt} \cdot \dot{\boldsymbol{x}}_{tt}, \tag{50}$$

where $\boldsymbol{J}_{tt} = \boldsymbol{J} \cdot \boldsymbol{J}_t$ is the 3×3 Jacobian matrix that reflects the relation between input and output velocities of a 3-PUU PKM, under the T-T angle convention.

4.3. The Principle of Virtual Work

Assume the virtual input displacement vector of three actuators referring to the actuator force vector $\boldsymbol{f}$ is $\delta \boldsymbol{h} = [\delta h_1, \delta h_2, \delta h_3]^T$, and the corresponding virtual output displacement vector is $\delta \boldsymbol{x}_{tt} = [\delta M_z, \delta \alpha, \delta \beta]^T$. Then, according to the Principle of Virtual Work, we can obtain the following equation:

$$\left(\boldsymbol{f}^T + \boldsymbol{G}_s^T - \boldsymbol{f}_s^T\right) \delta \boldsymbol{h} + \left(\boldsymbol{F}_e^T + \boldsymbol{G}_p^T - \boldsymbol{f}_p^T\right) \delta \boldsymbol{x}_{tt} = 0, \tag{51}$$

where $\boldsymbol{G}_s = \hat{m}_s g[1\ 1\ 1]^T$ denotes the gravity force of the sliders, $\boldsymbol{f}_s = \hat{m}_s[\ddot{h}_1\ \ddot{h}_2\ \ddot{h}_3]^T$ is the inertial force of three sliders, $\boldsymbol{F}_e^T = [F_z\ T_x\ T_y]^T$ represents the external forces and torques exerted on the moving platform, $\boldsymbol{G}_p^T = [\hat{m}_p g\ \ 0\ \ 0]^T$ is the gravitational force of the moving platform.

In addition, the inertial force vector of the moving platform can be expressed as

$$\boldsymbol{f}_p = \boldsymbol{M}_p \ddot{\boldsymbol{x}}_{tt}, \tag{52}$$

where $\boldsymbol{M}_p = \begin{bmatrix} \hat{m}_p & 0 \\ 0 & \hat{\boldsymbol{I}}_{xy} \end{bmatrix}$, and $\hat{\boldsymbol{I}}_{xy}$ denotes the top-left 2×2 sub-matrix of inertial matrix $\boldsymbol{I}_p$.

Differentiating both sides of Eq. (50) yields

$$\ddot{h} = \dot{\boldsymbol{J}}_{tt} \cdot \dot{\boldsymbol{x}}_{tt} + \boldsymbol{J}_{tt} \cdot \ddot{\boldsymbol{x}}_{tt}, \tag{53}$$

which is the corresponding inverse acceleration kinematics solution for the mechanism.

From Eq. (50), it's easy to obtain

$$\delta \boldsymbol{x}_{tt} = \boldsymbol{J}_{tt}^{-1} \cdot \delta \boldsymbol{h}. \tag{54}$$

Substituting Eq. (54) into Eq. (51) produces

$$\left(\boldsymbol{f}^T + \boldsymbol{G}_s^T - \boldsymbol{f}_s^T + \boldsymbol{F}_e^T \cdot \boldsymbol{J}_{tt}^{-1} + \boldsymbol{G}_p^T \cdot \boldsymbol{J}_{tt}^{-1} - \boldsymbol{f}_p^T \cdot \boldsymbol{J}_{tt}^{-1}\right) \delta \boldsymbol{h} = 0. \tag{55}$$

Therefore,

$$\boldsymbol{f}^T + \boldsymbol{G}_s^T - \boldsymbol{f}_s^T + \boldsymbol{F}_e^T \cdot \boldsymbol{J}_{tt}^{-1} + \boldsymbol{G}_p^T \cdot \boldsymbol{J}_{tt}^{-1} - \boldsymbol{f}_p^T \cdot \boldsymbol{J}_{tt}^{-1} = 0. \tag{56}$$

Assume there are no external forces and torques, i.e., $\boldsymbol{F}_e^T = 0$. By substituting Eq. (52) into Eq. (56) and taking the transpose of it, we can get

$$\boldsymbol{f} = -\boldsymbol{G}_s + \boldsymbol{f}_s - \left(\boldsymbol{J}_{tt}^{-1}\right)^T \cdot \boldsymbol{G}_p + \left(\boldsymbol{J}_{tt}^{-1}\right)^T \boldsymbol{M}_p \ddot{\boldsymbol{X}}, \tag{57}$$

which is the inverse dynamics solution of a 3-PUU mechanism produced by the Principle of Virtual Work. Notably, the Jacobian matrix utilized here is not limited to $\boldsymbol{J}_{tt}$ and can be $\boldsymbol{J}$ described in Eq.

https://doi.org/10.1017/S0263574716000692 Published online by Cambridge University Press

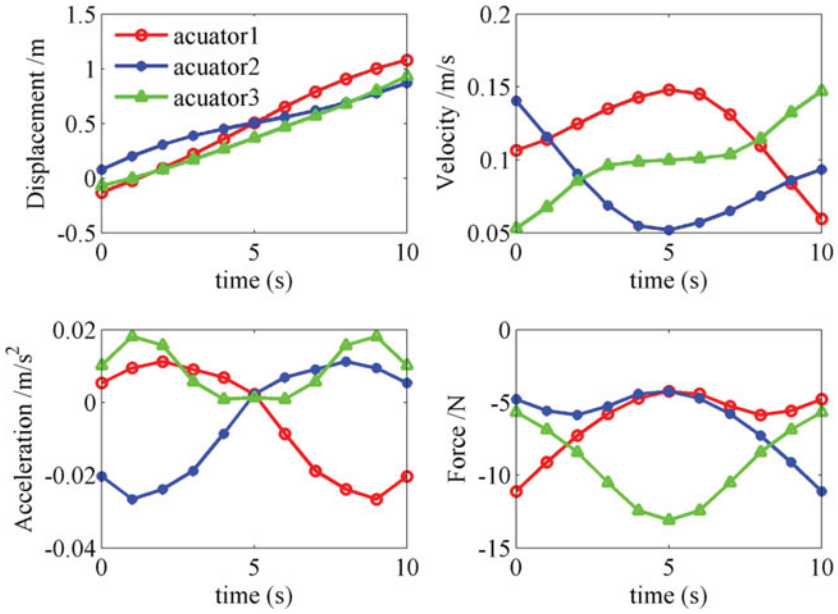

Fig. 5. Displacement, velocity, acceleration and actuated force of three actuators for 3-PUU mechanism.

(41). The T-T angle has been selected as it will be more convenient when expressing the helical path in the next subsection.

4.4. Dynamic simulation

Line path and circle path are the two most typical path types used in robot simulation research. Helical path combines them together, and it could reflect the dynamical features of a PKM very well. Thus, the helical path is widely used in dynamics analysis of PKMs.[1,2,9] Here, we let the moving platform track a helical path with the radius $r_{\text{helical}} = 20\,\text{mm}$, the pitch $h_{\text{helical}} = 10\,\text{mm}$, the angular frequency $\eta = \frac{\pi}{5}$ rad/s and $T = 10\,\text{s}$. The equation of the helical path with respect to the fixed frame is given as follows:

$$\begin{cases} x = r_{\text{helical}} \cdot \sin(\eta t) \\ y = r_{\text{helical}} \cdot \cos(\eta t) \\ z = z_0 + h_{\text{helical}} \cdot t \end{cases}, \tag{58}$$

where the starting height $z_0 = 460\,\text{mm}$.

A helical trajectory is hard to explicitly express with the ZXY Euler angle, whereas it is rather easy to be fulfilled with the T-T angle. Taking Eqs. (20), (47) and (58) into comprehensive consideration, we obtain

$$\begin{cases} \alpha = -\frac{1}{2}\eta t + \frac{\pi}{2} \\ \beta = \cos^{-1}\left(1 - \frac{2r_{\text{helical}}}{r}\right) \\ M_z = z_0 + h_{\text{helical}} \cdot t \end{cases}, \tag{59}$$

which is the analytical expression of the helical path under the T-T angle convention.

Based on Eqs. (29), (50), (53), (57) and (59), corresponding displacement, velocity, acceleration and actuated force of three actuators are calculated and depicted in Fig. 5.

The above helical path described by Eq. (59) is also tracked by a 3-PRS mechanism with the same architectural size and dynamical parameters, corresponding results are illustrated in Fig. 6. Notably, because the parasitic motion expression of 3-PRS and 3-PUU are different, the real helical paths tracked by them actually aren't the same one. To ensure that the two dynamics analysis results are more comparable in terms of dynamics features, we consciously hope the helical path tracked by the two mechanisms can be as close as possible.

https://doi.org/10.1017/S0263574716000692 Published online by Cambridge University Press

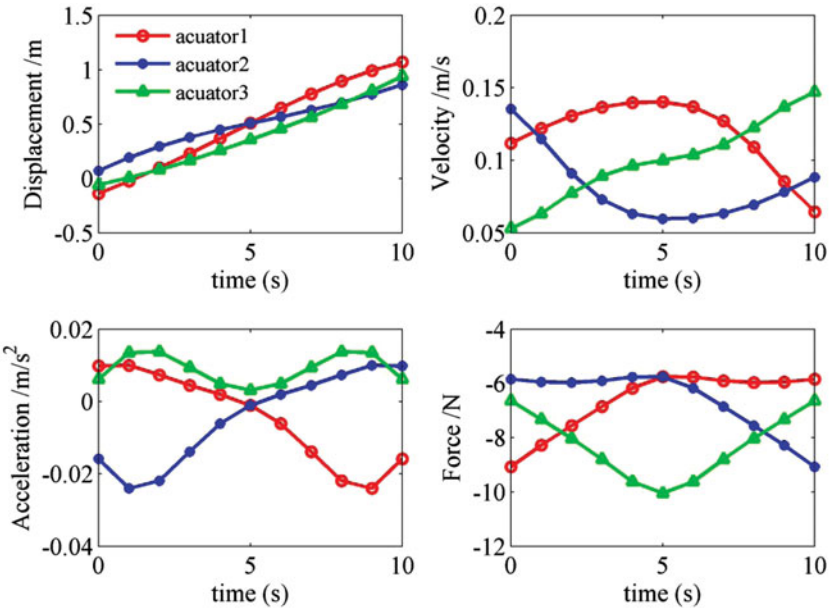

Fig. 6. Displacement, velocity, acceleration and actuated force of three actuators for 3-PRS mechanism.

By comparing Figs. 5 and 6, we can see that in this limiting case, there are only minor differences between these two mechanisms in terms of actuated displacement and velocity. This is mainly due to the fact that the ratio between r_{helical}, h_{helical} and R are very small, i.e., $\frac{1}{20}$ and $\frac{1}{40}$. Plus 3-PRS and 3-PUU share a similar layout structure, their displacement and velocity are almost identical. But after differential, obvious distinction starts to appear at the acceleration and actuator force simulation, where the maximum absolute value of actuator forces of 3-PUU is 13.09 N and that of 3-PRS is 10.04 N.

After acquiring displacement and force information, we can roughly calculate the actuated work with the numerical integration method:

$$W = \sum_{i=1}^{3} \sum_{j=2}^{n} \left(F_i^j + F_i^{j-1} \right) \left(d_i^j - d_i^{j-1} \right) /2, \tag{60}$$

where F_i^j denotes the actuated force of the ith limb at the jth integral step, and d_i^j denotes the actuated displacement of the ith limb at the jth integral step, n represents the whole integral steps number.

With Eq. (60), we are able to solve the actuated work provided by these two mechanisms while accomplishing helical path tracking. Interestingly, the two actuated work values are almost the same: 3-PUU costs 21.559997 J and 3-PRS costs 21.560005 J. The moving platforms of the two mechanisms own the same dynamical parameters and track the same path, thus the output work of the two mechanisms are also the same. With the same input work value and output work value, it's not hard to see that 3-PUU has the same energy transformation efficiency level as the widely-used 3-PRS mechanism.

In sum, although the maximum actuator force of 3-PUU in the example is about 30% higher than that of 3-PRS, 3-PUU share the same dynamics features as the 3-PRS in terms of energy transformation efficiency. Thus, from a dynamics perspective, the 3-PUU mechanism is undoubtedly suitable to be utilized as a machine tool head.

5. Conclusions

In this paper, we propose a parallel mechanism with 3-PUU structure. A detailed discussion about its architecture and geometry indicates that when projecting the 3-PUU scheme onto the Oxy plane,

https://doi.org/10.1017/S0263574716000692 Published online by Cambridge University Press

the projection of three linkages perpetually intersect at the projection of M point. On the basis of geometrical constraints, the parasitic motion of the moving platform is derived and explicitly expressed with the ZXY Euler angle convention. Then, the IKP, the Jacobian matrix calculation, and the FKP are investigated. Finally, with a simplified dynamics model, inverse dynamics analysis is carried out based on the Principle of Virtual Work, which illustrates that the 3-PUU mechanism has good dynamics features. In contrast, although the maximum actuator force of 3-PUU is about 30% higher than that of 3-PRS, 3-PUU share the same dynamics features of 3-PRS from the energy consumption perspective. These analyses in this paper validate the feasibility of applying this mechanism as a tool head module.

Acknowledgements

Support from the National Science Fund for Distinguished Young Scholars (Grant No.51225503) and Tsinghua University Initiative Scientific Research Program (No. 2014z22068) toward this paper is gratefully appreciated.

References

1. L.-W. Tsai, *Robot Analysis: The Mechanics of Serial and Parallel Manipulators*. (Wiley, New York, 1999).
2. J. P. Merlet, *Parallel Robots* (Springer, New York, 2005).
3. X.-J. Liu and J. Wang, *Parallel Kinematics: Type, Kinematics, and Optimal Design* (Springer, New York, 2013).
4. J. Wahl, Articulated Tool Head. WIPO Patent No. WO 00/25976; 2000.
5. F. Pierrot, C. Reynaud and A. Fournier, "Delta: A simple and efficient parallel robot," *Robotica* **8**(2), 105–109 (1990).
6. J. Han, Q. Huang and T. Chang, "Research on Space Docking HIL Simulation System Based on Stewart 6-DOF Motion System," *Proceedings of the 7th JFPS International Symposium on Fluid Power*, Toyama (2008) pp. 213–218.
7. L.-W. Tsai and S. Joshi, "Kinematic analysis of 3-DOF position mechanisms for use in hybrid kinematic machines," *Trans. ASME: J. Mech. Des.* **124**(2), 245–253 (2002).
8. M. S. Tsai and W. H. Yuan, "Dynamics modeling and decentralized control of a 3PRS parallel mechanism based on constrained robotic analysis," *J. Intell. Robot. Syst.* **63**(3), 525–545 (2011).
9. Y. Li and Q. Xu, "Kinematics and dynamics analysis for a general 3-PRS spatial parallel mechanism," *Robotica* **23**(2), 219–29 (2005).
10. M. S. Tsai and W. H. Yuan, "Inverse dynamics analysis for a 3-PRS parallel mechanism based on a special decomposition of the reaction forces," *Mech. Mach. Theory* **45**, 491–508 (2010).
11. Y. Li and Q Xu, "Kinematic analysis of a 3-PRS parallel manipulator," *Robot. Comput.-Integr. Manuf.* **23**(4), 395–408 (2007).
12. X.-J. Liu and I. A. Bonev, "Orientation capability, error analysis, and dimensional optimization of two articulated tool heads with parallel kinematics," *J. Manuf. Sci. Eng.* **130**(1), 011015-1–9 (2008).
13. G. Pond and J. A. Carretero, "Architecture optimization of three 3-PRS variants for parallel kinematic machining," *Robot. Comput.-Integr. Manuf.* **25**(1), 64–72 (2009).
14. Q. Li, Z. Chen, Q. Chen, C. Wu and X. Hu, "Parasitic motion comparison of 3-PRS parallel mechanism with different limb arrangement," *Robot. Comput.-Integr. Manuf.* **27**(2), 389–396 (2011).
15. T. Huang and H. T. Liu, "A parallel device having double rotation freedoms and one translation freedom," PCT Patent NO. WO 2007/124637.
16. X. Chen *et al.*, "A comparison study on motion/force transmissibility of two typical 3-DOF parallel manipulators: The Sprint Z3 and A3 tool heads," *Int. J. Adv. Robot. Syst.* **11**, 1–10 (2014).
17. Q. Li and J. M. Herve, "1T2R parallel mechanisms without parasitic motion," *IEEE Trans. Robot.* **26**, 401–410 (2010).
18. F. Xie, X.-J. Liu and J. Wang, "A 3-DOF parallel manufacturing module and its kinematic optimization," *Robot. Comput.-Integr. Manuf.* **28**(3), 334–343 (2012).
19. L.-W. Tsai, "Systematic enumeration of parallel manipulators," TR 1998-33, Institute for systems research, University of Maryland, USA, 1998.
20. L.-W. Tsai, *Mechanism Design: Enumeration of Kinematic Structures According to Function* (CRC Press, Boca Raton, 2000).
21. H. Giberti, P. Righettini and A. Tasora, "Design and Experimental Test of a Pneumatic Translational 3dof Parallel Manipulator," *Proceeding of the 10th International Workshop on Robotics in Alpe-Adria-Danube Region*, Vienna, Austria (May 16–18, 2001).
22. Y. Li and Q. Xu, "A new approach to the architecture optimization of a general 3-PUU translational parallel manipulator," *J. Intell. Robot. Syst.* **46**(1), 59–72 (2006).
23. Y. Li and Q. Xu, "Stiffness analysis for a 3-PUU PKM," *Mech. Mach. Theory* **43**, 186–200 (2008).

24. B. Dasgupta and T. S. Mruthyunjaya, "A newton-euler formulation for the inverse dynamics of the Stewart platform manipulator," *Mech. Mach. Theory* **33**(13), 1135–1152 (1998).
25. K.-M. Lee and D. K. Shah, "Dynamic analysis of a tree-degrees-of-freedom in-parallel actuated manipulator," *IEEE J. Robot. Autom.* **4**(3), 361–367 (1988).
26. B. Li, Z. Wang and J. Li, "Study on the dynamics of novel parallel mechanisms base on Kane's equation," *Mech. Sci. Technol. Aerospace Eng.* **18**(1), 41–43 (1999) (Chinese).
27. L.-W. Tsai, "Solving the inverse dynamics of a Stewart-Gough manipulator by the principle of virtual work," *J. Mech. Des.* **122**(1), 3–9 (2000).
28. Z. Huang, J. F. Liu and D. X. Zeng, "A general methodology for mobility analysis of mechanisms based on constraint screw theory," *Sci. China, Series E: Technol. Sci.*, **52**(5), 1337–1347 (2009).
29. J. S. Zhao, K. Zhou and Z. J. Feng, "A theory of degrees of freedom for mechanisms," *Mech. Mach. Theory* **39**, 621–643 (2004).
30. W. Liping, Xu Huayang and G. Liwen, "Mobility analysis of parallel mechanisms based on screw theory and mechanism topology," *Adv. Mech. Eng.* **7**(11), 1–13 (2015).
31. I. A. Bonev, Geometric Analysis of Parallel Mechanisms *Ph.D. Thesis* (Quebec, Canada: Laval University, 2002).